PHYSICAL REVIEW D **90,** 015005 (2014)

Top-mode pseudo-Nambu-Goldstone bosons at the LHC

Hidenori S. Fukano[1,*] and Shinya Matsuzaki[2,3,†]

[1]*Kobayashi-Maskawa Institute for the Origin of Particles and the Universe (KMI) Nagoya University, Nagoya 464-8602, Japan*

[2]*Institute for Advanced Research, Nagoya University, Nagoya 464-8602, Japan*

[3]*Department of Physics, Nagoya University, Nagoya 464-8602, Japan*

(Received 28 January 2014; published 3 July 2014)

We discuss LHC phenomenologies of the top-mode pseudo-Nambu-Goldstone bosons (pNGBs)(h_t^0, A_t^0), composite pNGBs predicted in the model recently proposed in a framework of the top-quark condensation. The *CP*-even top-mode pNGB, dubbed tHiggs (h_t^0), is identified with the 126 GeV Higgs boson at the LHC. We analyze the coupling properties of the tHiggs in comparison with the currently available data reported from LHC Run-I to find that the tHiggs can be consistent with the LHC Higgs boson. The mass formula relating masses of the top-mode pNGBs allows us to place an indirect limit on the mass of the *CP*-odd top-mode pNGBs (A_t^0) from the constraint on the tHiggs coupling strengths. The presence of the mass formula also significantly affects the coupling property of A_t^0, which ensures A_t^0 weakly coupled to the Standard Model particles. The direct limit on the mass of A_t^0 is placed by data on searches for new resonances in several channels at the LHC Run-I. We find the lower mass bound from both the indirect and direct limits, $m_{A_t^0} \gtrsim 560$ GeV. The discovery channel of A_t^0 in the upcoming LHC Run-II is also addressed.

DOI: 10.1103/PhysRevD.90.015005 PACS numbers: 14.80.Ec, 12.60.Rc

I. INTRODUCTION

A 126 GeV Higgs boson has been discovered at the LHC (so-called LHC Run-I) by the ATLAS [1] and CMS experiments [2]. It has so far been reported that the LHC Higgs boson has the properties compatible with the Higgs boson in the Standard Model (SM). After the discovery of the 126 GeV Higgs boson, one of the primary targets for future collider experiments such as the upcoming next LHC run (LHC Run-II) is to reveal the dynamical origin of the Higgs boson responsible for the mass generation of the SM particles and discover the related new particles beyond the SM.

One key hint at accessing such a dynamical origin of the Higgs boson would be deduced from an observed coincidence among scales of top-quark, Higgs boson, and weak gauge boson masses; of the SM particles, they are the only ones roughly on the same order. Top-quark condensation [3–8] naturally provides such a close relation between those mass scales. The top-quark condensate model was proposed [3,4] to predict the top-quark mass to be on the order of the electroweak symmetry breaking scale, which was before the discovery of the top quark. However, the original top-quark condensate model is somewhat far from a realistic situation; the predicted value of the top quark mass is too large compared to the experimental value. In addition, a Higgs boson predicted as a $t\bar{t}$ bound state has the mass in a range of $m_t < m_H < 2m_t$, which cannot be identified with the 126 GeV Higgs boson at the LHC.

Recently, a new class of the top-quark condensate model was proposed [9],[1] where the realistic top-quark mass is obtained by the top-seesaw mechanism [11,12] and a composite Higgs boson emerges as a pseudo-Nambu-Goldstone boson (pNGB) associated with the spontaneous breaking of a global symmetry, which can be as light as the 126 GeV Higgs boson at the LHC. The model in Ref. [9] is constructed from the top and bottom quarks $q = (t, b)$ and a (vectorlike) χ-quark, a flavor partner of the top quark having the same SM charges as those of the right-handed top quark, which form a four-fermion interaction, $G_{4f}(\bar{\psi}_L^i \chi_R)(\bar{\chi}_R \psi_L^i)$, where $\psi_L^i \equiv (t_L, b_L, \chi_L)^{Ti} (i = 1, 2, 3)$. The model possesses a global symmetry $U(3)_L \times U(1)_{\chi_R}$, which is spontaneously broken down to $U(2)_L \times U(1)_{L+\chi_R}$ by the quark condensations $\langle \bar{\chi}_R t_L \rangle \neq 0$ and $\langle \bar{\chi}_R \chi_L \rangle \neq 0$, triggered by the supercritical four-fermion coupling $G_{4f} > G_{\rm crit}$, where $G_{\rm crit}$ is the critical coupling. The associated five Nambu-Goldstone bosons (NGBs) emerge as bound states of the quarks, in addition to a composite heavy Higgs boson corresponding to the σ mode of the usual Nambu–Jona-Lasinio (NJL) model [13].

Three of those NGBs are eaten by the electroweak gauge bosons when the subgroup of the symmetry is gauged by the electroweak symmetry, while two of them become pNGBs and remain as physical states, dubbed "top-mode pNGBs." Those two top-mode pNGBs acquire their masses due to additional terms that explicitly break the $U(3)_L \times U(1)_{\chi_R}$ symmetry in such a way that the vacuum aligns to

*fukano@kmi.nagoya-u.ac.jp
†synya@hken.phys.nagoya-u.ac.jp

[1]At almost the same time as Ref. [9], a similar model was proposed in a slightly different context [10].

break the electroweak symmetry by $\langle \bar{\chi}_R t_L \rangle \neq 0$. One of them is a *CP*-even scalar, "tHiggs" (h_t^0), which is identified as the 126 GeV Higgs boson at the LHC, while the other one is a *CP*-odd scalar (A_t^0) having the same quantum number as that of other *CP*-odd scalars as in the minimal supersymmetric Standard Model (MSSM) and the two-Higgs doublet model (2HDM). These two top-mode pNGBs are expected to be the low-lying spectra, and the *CP*-odd scalar A_t^0 will be a new particle, which can be the phenomenological consequence for the model to be tested at the LHC.

The model in Ref. [9] predicts a notable relation between masses of two top-mode pNGBs at the tree level,

$$m_{h_t^0}^{(0)} = m_{A_t^0}^{(0)} \sin\theta,$$

where the angle θ is a model parameter related to the presence of the condensate, $\langle \bar{\chi}_R q_L \rangle \neq 0$, which causes the electroweak symmetry breaking. The above mass formula is established at the tree level of the perturbation with respect to couplings explicitly breaking the $U(3)_L \times U(1)_{\chi_R}$ symmetry. The next-to-leading-order corrections, especially coming from terms introduced to generate the top-quark mass, gives rise to significant corrections to the h_t^0 mass, so that the tree-level h_t^0 mass is set so as to realize the mass at around 126 GeV at the one-loop level, say, $m_{h_t^0}^{(0)} \simeq 230$ GeV [9] [see also Eq. (26)]. On the other hand, the A_t^0 mass does not get large corrections [9], and hence the one-loop mass is almost the same as the tree-level one, $m_{A_t^0} \simeq m_{A_t^0}^{(0)}$ [see Eq. (27)].

The angle θ in the above formula also controls the size of deviation of the tHiggs couplings from the SM Higgs ones [9]:

$$\frac{g_{h_t^0 VV}}{g_{h_{\rm SM} VV}} = \frac{g_{h_t^0 bb}}{g_{h_{\rm SM} bb}} = \frac{g_{h_t^0 \tau\tau}}{g_{h_{\rm SM}\tau\tau}} = \cos\theta, \qquad \frac{g_{h_t^0 tt}}{g_{h_{\rm SM} tt}} = \frac{2\cos^2\theta - 1}{\cos\theta}.$$

Note that the tHiggs couplings to the SM particles coincide with those of the SM Higgs boson in an extreme limit $\sin\theta \to 0$. In this limit, one can see from the above mass formula that $m_{A_t^0}^{(0)}/m_{h_t^0}^{(0)} \to \infty$, implying decoupling of the A_t^0 from the theory. Thus, precise measurements of deviation from the SM Higgs couplings would be a crucial key for the presence of A_t^0 having the mass within the reach of the LHC search and would also place an indirect bound on the A_t^0 mass, in addition to the limits from the direct searches for A_t^0 at the LHC.

In this paper, we discuss LHC phenomenologies of the top-mode pNGBs (h_t^0, A_t^0) predicted in the model of Ref. [9]. Identifying the *CP*-even top-mode pNGB (tHiggs, h_t^0) with the 126 GeV Higgs boson at the LHC, we analyze the coupling properties of the tHiggs and compare them with the currently available data on the Higgs coupling measurements reported from LHC Run-I [14–24]. We evaluate the constraint on the tHiggs couplings to the SM particles to find that the tHiggs can be consistent with the LHC Higgs boson, allowing a size of the deviation (controlled by $\cos\theta$) from the SM Higgs couplings. An indirect limit on the mass of *CP*-odd top-mode pNGB (A_t^0) is set through the mass formula ($\sin\theta = m_{h_t^0}^{(0)}/m_{A_t^0}^{(0)} \simeq m_{h_t^0}^{(0)}/m_{A_t^0}$) to be $m_{A_t^0} \geq 563$ GeV.

We then calculate the production cross sections and partial decay widths of A_t^0 relevant to the LHC study and find that A_t^0 is dominantly produced via the gluon-gluon fusion process and mainly decays to gg and Zh_t^0 for a low-mass range, 563 GeV $\leq m_{A_t^0} \leq 1$ TeV, and $t\bar{t}$, gg for a high mass range, $m_{A_t^0} > 1$ TeV. The total width of A_t^0 is shown to be quite smaller than that of the SM Higgs boson and other *CP*-odd scalars like A^0 as in the MSSM/2HDM. This is due to the presence of the mass formula displayed above, which is intrinsic to the top-mode pNGBs; the mass formula ensures A_t^0 weakly coupled to the SM particles. Furthermore, we place a direct mass bound on A_t^0 from the LHC Run-I data on direct searches for new resonances in several channels. We then find all the direct limits are milder than the indirect limit.

The discovery channel of A_t^0 in the upcoming LHC Run-II is also addressed; a heavy A_t^0 with the mass $m_{A_t^0} \geq 1$ TeV can be seen as a quite narrow resonance in the $A_t^0 \to t\bar{t}$ or $A_t^0 \to gg$ channel, while a light A_t^0 with the mass in a range 563 GeV $\leq m_{A_t^0} \leq 1$ TeV may be measured via $A_t^0 \to Zh_t^0$, which would be earlier than the discovery of other *CP*-odd scalars.

This paper is organized as follows. In Sec. II, we give a brief review of a phenomenological Lagrangian describing the top-mode pNGBs (h_t^0, A_t^0) based on the $[U(3)_L \times U(1)_{\chi_R}]/[U(2)_L \times U(1)_{L+\chi_R}]$ nonlinear sigma model [9]. In Sec. III, the coupling properties of h_t^0 are discussed in comparison with the currently available data from the Higgs coupling measurements at the LHC Run-I, and then we convert the result into the constraint on the mass of A_t^0 through the mass formula mentioned above. In Sec. IV, we compute the partial decay widths and production cross sections of A_t^0 relevant to the LHC study. The limits on the A_t^0 mass are then placed from the LHC Run-I data on direct searches for new resonances in several channels currently reported by the ATLAS and CMS experiments. The discovery channel of A_t^0 is also addressed in light of the upcoming LHC Run-II. Section V is devoted to the summary of this paper.

II. PHENOMENOLOGICAL LAGRANGIAN FOR THE TOP-MODE pNGBs

In this section, we review a low-energy effective Lagrangian relevant to studying the LHC phenomenologies of the top-mode pNGBs [9]. The model proposed in

Ref. [9] consists of the top and bottom quarks $q^3 = (t, b)$ and a (vectorlike) χ quark, which is a flavor partner of the top quark having the same SM charges as those of the right-handed top quark. In addition to the kinetic term of those quarks, the model includes a four-fermion interaction $G_{4f}(\bar{\psi}^i_L\chi_R)(\bar{\chi}_R\psi^i_L)$, where $\psi^i_L \equiv (q^3_L, \chi_L)^{Ti} = ((t_L, b_L), \chi_L)^{Ti} (i = 1, 2, 3)$. The model then possesses a global symmetry $U(3)_L \times U(1)_{\chi_R}$ that is spontaneously broken down to $U(2)_L \times U(1)_{L+\chi_R}$ by the quark condensations $\langle \bar{\chi}_R t_L \rangle \neq 0$ and $\langle \bar{\chi}_R \chi_L \rangle \neq 0$, triggered by the supercritical four-fermion coupling $G_{4f} > G_{\rm crit}$, where $G_{\rm crit}$ is the critical coupling.

As discussed in Ref. [9], the structure of the symmetry-breaking pattern of the model is actually twisted; the gap equation derived from the four-fermion dynamics has a rotational invariance with respect to the fermion dynamical masses associated with the condensates $\langle \bar{\chi}_R t_L \rangle \neq 0$ and $\langle \bar{\chi}_R \chi_L \rangle \neq 0$, which corresponds to changing the basis of the left-handed quarks from the electroweak gauge base to a flavor base as $\tilde{\psi}_L = R(\theta) \cdot \psi_L$ by the orthogonal rotation of $R(\theta)$. The symmetry-breaking pattern thus looks like $U(3)_{\tilde{\psi}_L} \times U(1)_{\chi_R} \to U(2)_{\tilde{\psi}_L} \times U(1)_{\tilde{\psi}_L + \chi_R}$. The associated five NGBs emerge as bound states of the quarks, in addition to a composite heavy Higgs boson (H^0_t) corresponding to the σ mode of the usual NJL model. Three of the NGBs are eaten by the W and Z bosons when the electroweak gauge is turnd on, while the other two become massive due to some explicit breaking effects, which we call the top-mode pNGBs.

Below the heavy composite Higgs mass scale (of $\mathcal{O}(1)$ TeV [9]), the model can be described by a nonlinear sigma model based on the coset space $G/H = [U(3)_{\tilde{\psi}_L} \times U(1)_{\chi_R}]/[U(2)_{\tilde{\psi}_L} \times U(1)_{\tilde{\psi}_L + \chi_R}]$. The representatives of the G/H parametrized by NGB fields π^a_t $(a = 4, 5, 6, 7, A)$ are

$$\xi_L = \exp\left[-\frac{i}{f}\left(\sum_{a=4,5,6,7} \pi^a_t \lambda^a + \frac{\pi^A_t}{2\sqrt{2}}\lambda^A\right)\right],$$
$$\xi_R = \exp\left[\frac{i}{f}\frac{\pi^A_t}{2\sqrt{2}}\lambda^A\right],$$

where f is the decay constant associated with the spontaneous breaking G/H, λ^a denotes the Gell-Mann matrices, and

$$\lambda^A = \begin{pmatrix} 0 & 0 & 0 \\ 0 & 0 & 0 \\ 0 & 0 & \sqrt{2} \end{pmatrix}.$$

It is convenient to further introduce the "chiral" field U as

$$U = \xi^\dagger_L \cdot \Sigma \cdot \xi_R \quad \text{with} \quad \Sigma = \frac{1}{\sqrt{2}}\lambda^A. \tag{1}$$

The transformation properties of $\xi_{L,R}$ and U under G are given by

$$\xi_L \to h(\pi_t, \tilde{g}) \cdot \xi_L \cdot g^\dagger_{3\tilde{L}}, \qquad \xi_R \to h(\pi_t, \tilde{g}) \cdot \xi_R \cdot g^\dagger_{1R},$$
$$U \to g_{3\tilde{L}} \cdot U \cdot g^\dagger_{1R}, \tag{2}$$

where $\tilde{g} = \{g_{3\tilde{L}}, g_{1R}\}, g_{3\tilde{L}} \in U(3)_{\tilde{\psi}_L}, g_{1R} \in U(1)_{\chi_R}$, and $h(\pi_t, \tilde{g}) \in H$. The G-invariant Lagrangian is thus constructed in terms of the NGBs to the lowest order of derivatives as

$$\frac{f^2}{2}\,\mathrm{tr}[\partial_\mu U^\dagger \partial^\mu U]. \tag{3}$$

When the electroweak symmetry is turned on, the covariant derivative acting on U is given by

$$D_\mu U \equiv R(\theta)\left[\partial_\mu - ig\sum_{a=1}^{3} W^a_\mu \left(\begin{array}{cc|c} & & 0 \\ & \tau^a/2 & 0 \\ \hline 0 & 0 & 0 \end{array}\right) + ig' B_\mu \begin{pmatrix} 1/2 & 0 & 0 \\ 0 & 1/2 & 0 \\ 0 & 0 & 0 \end{pmatrix}\right] R^T(\theta) \cdot U,$$
$$R(\theta) = \begin{pmatrix} \cos\theta & 0 & -\sin\theta \\ 0 & 1 & 0 \\ \sin\theta & 0 & \cos\theta \end{pmatrix}, \tag{4}$$

where W_μ and B_μ are the $SU(2)_L$ and $U(1)_Y$ gauge boson fields with the gauge couplings g and g', respectively. Thus, the Lagrangian Eq. (3) is changed to the covariant form

$$\mathcal{L}_{\rm NL\sigma M} = \frac{f^2}{2}\,\mathrm{tr}[D_\mu U^\dagger D^\mu U]. \tag{5}$$

The NGBs $(z^0_t, w^\pm_t) \equiv (\pi^4_t \cos\theta + \pi^A_t \sin\theta, (\pi^6_t \mp i\pi^7_t)/\sqrt{2})$ are then eaten by the Z and W bosons, leading to the Z and W masses,

$$m^2_Z = \frac{1}{4}(g^2 + g'^2) f^2 \sin^2\theta, \qquad m^2_W = \frac{1}{4} g^2 f^2 \sin^2\theta.$$

These mass formulas imply

$$v^2_{\rm EW} = f^2 \sin^2\theta, \tag{6}$$

which is set by the Fermi constant G_F as $v_{\rm EW} = (\sqrt{2}G_F)^{-1/2} \simeq 246$ GeV [25]. As seen from Eq. (6), the nonzero angle θ $(\sin\theta)$, rotating left-handed fermions in the gauge (ψ_L) and flavor $(\tilde{\psi}_L)$ bases, dictates the electroweak

symmetry breaking ($v_{\rm EW}$) and hence is related to the vacuum alignment problem.[2]

The remaining two NGBs $(h_t^0, A_t^0) \equiv (\pi^5, -\pi_t^4 \sin\theta + \pi_t^A \cos\theta)$ will become pNGBs (top-mode pNGBs) through explicit breaking terms introduced appropriately to the underlying four-fermion dynamics [9],

$$\Delta\mathcal{L}_{\rm NL\sigma M} = f^2 {\rm tr}[c_1 (R^T U)^\dagger \chi_1 (R^T U) + c_2 (\chi_2^\dagger (R^T U) + (R^T U)^\dagger \chi_2)], \tag{7}$$

where the spurion fields χ_1 and χ_2 transform under the G symmetry as

$$\chi_1 \to g_{3\tilde{L}} \cdot \chi_1 \cdot g_{3\tilde{L}}^\dagger, \qquad \chi_2 \to g_{3\tilde{L}} \cdot \chi_2 \cdot g_{1R}^\dagger. \tag{8}$$

The G symmetry is explicitly broken when the spurion fields acquire the vacuum expectation values,

$$\langle \chi_1 \rangle = \langle \chi_2 \rangle = \Sigma, \tag{9}$$

so that the c_1 and c_2 terms break the G down to $U(2)_{q_L^3} \times U(1)_{\chi_L} \times U(1)_{\chi_R}$ and $U(2)_{q_L^3} \times U(1)_{V=\chi_R+\chi_L}$. The coefficients c_1 and c_2 in Eq. (7) are fixed so as to give the mass formula between two top-mode pNGBs at the tree level of the perturbation with respect to the explicit breaking couplings [9],

$$m_{h_t^0}^{(0)} = m_{A_t^0}^{(0)} \sin\theta, \tag{10}$$

so that

$$c_1 = -\frac{1}{2}(m_{A_t^0}^{(0)})^2, \qquad c_2 = \frac{1}{2}(m_{A_t^0}^{(0)})^2 \cos\theta.$$

To describe interactions between fermions and the top-mode pNGBs, we may add the top- and χ-quark sectors to the nonlinear Lagrangian [9],

$$\mathcal{L}_{\rm yuk.}^{t,t'} = -\frac{f}{\sqrt{2}}[y\bar{\psi}_L (R^T U)\psi_R + y_{\chi t}\bar{\psi}_L (\chi_1 R^T U \chi_3)\psi_R + {\rm h.c.}], \tag{11}$$

where $\psi_R = (q_R^3, \chi_R)^T = ((t_R, b_R), \chi_R)^T$. The spurion fields χ_1 and χ_3 have been introduced in Eq. (11) and transform as

$$\chi_1 \to g_{3L} \cdot \chi_1 \cdot g_{3L}^\dagger, \qquad \chi_3 \to g_{1R} \cdot \chi_3 \cdot g_{1R}^\dagger, \tag{12}$$

so that the Lagrangian Eq. (11) is invariant under the G symmetry, $U(3)_{\tilde{\psi}_L} \times U(1)_{\chi_R}$, and $U(2)_{q_R^3}$ symmetry. These symmetries are explicitly broken by the vacuum expectation values of the spurion fields,

$$\langle \chi_1 \rangle = \Sigma, \qquad \langle \chi_3 \rangle = \lambda_4, \tag{13}$$

in which the $\langle \chi_1 \rangle$ breaks the $U(3)_{\psi_L}$ symmetry down to $U(2)_{\psi_L} \times U(1)_{\chi_L}$ and the $\langle \chi_3 \rangle$ breaks the $U(2)_{q_R^3} \times U(1)_{\chi_R}$ down to $U(1)_{\chi_R = t_R}$. Equation (11) gives the fermion mass matrix of seesaw type to be diagonalized by an orthogonal rotation as

$$\begin{aligned} &-(\bar{t}_L \quad \bar{\chi}_L)_g \begin{pmatrix} 0 & m_{t\chi} \\ \mu_{\chi t} & m_{\chi\chi} \end{pmatrix} \begin{pmatrix} t_R \\ \chi_R \end{pmatrix}_g + {\rm h.c.} \\ &= -(\bar{t}_L \quad \bar{t}'_L)_m \begin{pmatrix} m_t & 0 \\ 0 & m'_t \end{pmatrix} \begin{pmatrix} t_R \\ t'_R \end{pmatrix}_m + {\rm h.c.}, \end{aligned} \tag{14}$$

where $m_{t\chi}, \mu_{\chi t}$, and $m_{\chi\chi}$ can be expressed as a function of $y, y_{\chi t}$, and f and the subscripts g and m imply the gauge (current) and mass eigenstates, respectively, which are related by the orthogonal rotation,

$$\begin{aligned} \begin{pmatrix} t_L \\ t'_L \end{pmatrix}_m &= \begin{pmatrix} c_L^t & -s_L^t \\ s_L^t & c_L^t \end{pmatrix} \begin{pmatrix} t_L \\ \chi_L \end{pmatrix}_g, \\ \begin{pmatrix} t_R \\ t'_R \end{pmatrix}_m &= \begin{pmatrix} -c_R^t & s_R^t \\ s_R^t & c_R^t \end{pmatrix} \begin{pmatrix} t_R \\ \chi_R \end{pmatrix}_g, \end{aligned} \tag{15}$$

with $c_{L(R)}^t \equiv \cos\theta_{L(R)}^t$ and $s_{L(R)}^t \equiv \sin\theta_{L(R)}^t$. The explicit expressions for the mass eigenvalues $(m_t, m_{t'})$ can be found in Ref. [9], and we will not display them here since they are irrelevant to the present study. We shall take $y_{\chi t}/y < 1$ in order to realize the top-seesaw mechanism [11,12], which turns out to be consistent also with the constraint on the t'-quark mass from the electroweak precision tests [9]. The angles $c_{L(R)}^t$ and $s_{L(R)}^t$ can then be expanded in powers of $y_{\chi t}/y$ to be expressed up to $\mathcal{O}(y_{\chi t}^3/y^3)$ as

$$\begin{aligned} c_L^t &= \frac{1}{\sqrt{2}}\left[1 + \frac{m_{\chi\chi}^2 - m_{t\chi}^2 + \mu_{\chi t}^2}{m_{t'}^2 - m_t^2}\right]^{1/2} \\ &\simeq \cos\theta\left[1 + \frac{y_{\chi t}^2}{y^2}\cos^2\theta\sin^2\theta\right], \end{aligned} \tag{16}$$

$$\begin{aligned} s_L^t &= \frac{1}{\sqrt{2}}\left[1 - \frac{m_{\chi\chi}^2 - m_{t\chi}^2 + \mu_{\chi t}^2}{m_{t'}^2 - m_t^2}\right]^{1/2} \\ &\simeq \sin\theta\left[1 - \frac{y_{\chi t}^2}{y^2}\cos^4\theta\right], \end{aligned} \tag{17}$$

[2]As was noted in Ref. [9], the criticality $G_{4f} > G_{\rm crit}$ implies the R-rotational-invariant condensation, $\langle \bar{\chi}_R t_L \rangle^2 + \langle \bar{\chi}_R \chi_L \rangle^2 \neq 0$, but not necessarily $\langle \bar{\chi}_R t_L \rangle \neq 0$, which is responsible for the electroweak symmetry breaking. The electroweak gauge interaction itself can contribute to lifting the degeneracy between the vacuum with $\langle \bar{\chi}_R t_L \rangle = 0$ and that with $\langle \bar{\chi}_R t_L \rangle \neq 0$, which in principle would require some extreme fine-tuning of the critical coupling as well as the angle θ and some explicit breaking parameters (G' and G'' as introduced in Ref. [9]). The explicit analysis on the vacuum alignment will be pursued in another publication.

$$c_R^t = \frac{1}{\sqrt{2}}\left[1+\frac{m_{\chi\chi}^2+m_{t\chi}^2-\mu_{\chi t}^2}{m_{t'}^2-m_t^2}\right]^{1/2} \simeq 1-\frac{1}{2}\frac{y_{\chi t}^2}{y^2}\cos^4\theta, \quad (18)$$

$$s_R^t = \frac{1}{\sqrt{2}}\left[1-\frac{m_{\chi\chi}^2+m_{t\chi}^2-\mu_{\chi t}^2}{m_{t'}^2-m_t^2}\right]^{1/2} \simeq \frac{y_{\chi t}}{y}\cos^2\theta\left[1-\frac{1}{2}\frac{y_{\chi t}^2}{y^2}\cos^2\theta(\cos^2\theta-2\sin^2\theta)\right]. \quad (19)$$

As discussed in Ref. [9], the SM fermions other than the top quark are also allowed to acquire the masses and couple to the top-mode pNGBs by introducing some four-fermion interactions communicating with top and χ quarks, through the nonzero condensate $\langle\bar{\chi}_R t_L\rangle$, without invoking other condensations like bottom condensation. In terms of the nonlinear sigma model, such four-fermion terms can be replaced with the Yukawa interaction terms

$$\mathcal{L}_{\text{yuk.}}^{\text{others}} = -\frac{f}{\sqrt{2}}\left[\sum_{\alpha=1,2} y_{u^\alpha}\bar{\psi}_L^\alpha(\chi_4 R^T U\chi_5)\psi_R^\alpha - \sum_{\alpha=1,2,3} i y_{d^\alpha}\bar{\psi}_L^\alpha(\chi_6 R^T U\chi_7)\psi_R^\alpha + \sum_{\alpha=1,2,3} i y_{l^\alpha}\bar{l}_L^\alpha(\chi_6 R^T U\chi_7) l_R^\alpha + \text{h.c.}\right], \quad (20)$$

where $\psi_{L,R}^\alpha = (q_{L,R}^\alpha, 0)^T = ((u_{L,R}^\alpha, d_{L,R}^\alpha), 0)^T$ and $l_{L,R}^\alpha = (\nu_{L,R}^\alpha, e_{L,R}^\alpha, 0)^T$. The spurion fields $\chi_{4,5,6,7}$ have been introduced so as to make the Lagrangian invariant under the G. They have the vacuum expectation values

$$\langle\chi_4\rangle = \begin{pmatrix} 1 & 0 & 0 \\ 0 & 1 & 0 \\ 0 & 0 & 0 \end{pmatrix}, \qquad \langle\chi_5\rangle = \lambda_4, \qquad \langle\chi_6\rangle = \lambda_2, \qquad \langle\chi_7\rangle = \lambda_6. \quad (21)$$

From Eq. (20), the light SM fermions get masses as $m_{u^\alpha} = y_{u^\alpha}/\sqrt{2}v_{\text{EW}}, m_{d^\alpha} = y_{d^\alpha}/\sqrt{2}v_{\text{EW}}$, and $m_{e^\alpha} = y_{l^\alpha}/\sqrt{2}v_{\text{EW}}$, where use has been made of Eq. (6). In addition, we find the Yukawa couplings to the top-mode pNGBs:

$$\mathcal{L}_{\text{yuk.}}^{\text{others}} \ni -\cos\theta\left[\sum_{\alpha=1,2}\frac{m_{u^\alpha}}{v_{\text{EW}}} h_t^0 \bar{u}^\alpha u^\alpha + \sum_{\alpha=1,2,3}\frac{m_{d^\alpha}}{v_{\text{EW}}} h_t^0 \bar{d}^\alpha d^\alpha + \sum_{\alpha=1,2,3}\frac{m_{e^\alpha}}{v_{\text{EW}}} h_t^0 \bar{e}^\alpha e^\alpha\right]. \quad (22)$$

Note the absence of Yukawa couplings to the CP-odd top-mode pNGB A_t^0 for the light SM fermions, due to the orthogonality of the associated A_t^0 current to the SM light fermion currents. This implies that the A_t^0 cannot be produced through the Drell—Yan process or decay to $\tau^+\tau^-$ and $b\bar{b}$. The former in particular leads to no interference in searches for the SM-like Higgs produced with the Z boson, i.e., $q\bar{q} \to Zh$, in sharp contrast to other CP-odd Higgs bosons such as those in the 2HDM.

Thus, the phenomenological Lagrangian for the top-mode pNGBs is given by

$$\mathcal{L} = \mathcal{L}_{\text{NL}\sigma\text{M}} + \Delta\mathcal{L}_{\text{NL}\sigma\text{M}} + \mathcal{L}_{\text{yuk.}}^{t,t'} + \mathcal{L}_{\text{yuk.}}^{\text{others}}[\text{Eq. (22)}]. \quad (23)$$

In the following sections, we will employ the LHC phenomenologies of the top-mode pNGBs based on the Lagrangian Eq. (23).

Before proceeding to the LHC phenomenology, we shall remark on the radiative corrections to the top-mode pNGB masses, arising as the next-to-leading-order terms in the perturbation with respect to the explicit breaking parameters $c_{1,2}, y_{\chi t}$ in $\Delta\mathcal{L}_{\text{NL}\sigma M}$ and $\mathcal{L}_{\text{yuk.}}^{t,t'}$. Of these corrections at the one-loop order, the top and t' loop arising as terms of $\mathcal{O}(y_{\chi t}^2) \sim \mathcal{O}(m_t^2/v_{\text{EW}}^2)$ will give the most sizable contributions [9]. However, we may integrate out the t' quark so as not to incorporate the loop contribution to the top-mode pNGB masses; recall the relationship between the masses of the χ quark and the heavy Higgs, which is set by the usual formula derived from the NJL dynamics, $m_{H_t^0} = 2m_{\tilde{\chi}\chi}$, where $m_{\tilde{\chi}\chi} = \sqrt{m_{\chi\chi}^2+m_{t\chi}^2}$. As it will turn out, the t' quark is required to be almost composed from the χ quark with s_L^t in Eq. (17) being approximated to be $\sim\sin\theta < 0.3$ to be consistent with the Higgs coupling measurement at the LHC Run-I [see Eqs. (40) and (42)]. Hence, we may take $m_{t'} \sim m_{\tilde{\chi}\chi}$, which is quite close to the heavy Higgs mass scale, i.e., the cutoff scale of the nonlinear sigma model. We may thus integrate out the t' quark and take the t'-quark mass to be the cutoff of the effective theory. In that case, the mass shifts of two top-mode pNGB masses are given by [9]

$$m_{h_t^0}^2 = (m_{h_t^0}^{(0)})^2 - \frac{3m_{t'}^2}{8\pi^2}\left(\frac{\sqrt{2}m_t}{v_{\text{EW}}}\right)^2 \frac{1-6\cos^2\theta+6\cos^4\theta}{\cos^2\theta} \times\left[1+\mathcal{O}\left(\frac{y_{\chi t}^2}{y^2}\right)\right], \quad (24)$$

$$m_{A_t^0}^2 = (m_{A_t^0}^{(0)})^2 - \frac{3m_{t'}^2}{8\pi^2}\left(\frac{\sqrt{2}m_t}{v_{\text{EW}}}\right)^2 \times\frac{(1-\cos^2\theta)(2-7\cos^2\theta+6\cos^4\theta)}{2\cos^2\theta}\left[1+\mathcal{O}\left(\frac{y_{\chi t}^2}{y^2}\right)\right]. \quad (25)$$

From these, we see that setting the tHiggs mass at one-loop level $m_{h_t^0} = 126$ GeV requires the tree-level mass to be

$$m_{h_t^0}^{(0)} \simeq 230\ \text{GeV}, \tag{26}$$

for $m_{t'} \simeq 1.2$ TeV, $y_{\chi t}/y \simeq 0.7$, and $\cos\theta \sim 0.97$, which is consistent with the Higgs coupling measurement, as will be seen later, and the S, T parameter constraint [9]. Note, on the other hand, that the A_t^0 mass is almost stable against the top-quark loop for $\cos\theta \sim 1$:

$$m_{A_t^0} \simeq m_{A_t^0}^{(0)}. \tag{27}$$

III. *CP*-EVEN TOP-MODE pNGB (tHIGGS h_t^0) AT THE LHC

In this section, we discuss the coupling properties of the tHiggs h_t^0 with $m_{h_t^0} = 126$ GeV in comparison with the currently available Higgs search data at the LHC. We further place the limit on the mass of A_t^0 by using the mass relation between two top-mode pNGBs, Eq. (10).

A. tHiggs coupling properties

After the t' quark is integrated out by assuming $m_{t'} \gg m_{t,h_t^0,A_t^0}$, the relevant tHiggs interaction terms are read off from the Lagrangian Eq. (23),

$$\mathcal{L}_{h_t^0} = g_{hVV}\frac{v_{\rm EW}}{2}\left(g^2 h_t^0 W_\mu^+ W^{-\mu} + \frac{g^2+g'^2}{2} h_t^0 Z_\mu Z^\mu\right) - g_{htt}\frac{m_t}{v_{\rm EW}} h_t^0 \bar{t}t - g_{hbb}\frac{m_b}{v_{\rm EW}} h_t^0 \bar{b}b - g_{h\tau\tau}\frac{m_\tau}{v_{\rm EW}} h_t^0 \bar{\tau}\tau, \tag{28}$$

where

$$g_{hVV} = g_{hbb} = g_{h\tau\tau} = \cos\theta, \tag{29}$$

$$g_{htt} = \frac{v_{\rm EW}}{m_t}\frac{y}{\sqrt{2}}\left[(c_L^t \cos\theta + s_L^t \sin\theta)s_R^t - s_L^t c_R^t \sin\theta\left(\frac{y_{\chi t}}{y}\right)\right] = \frac{2\cos^2\theta - 1}{\cos\theta} + \mathcal{O}\left(\frac{y_{\chi t}^2 \sin^2\theta}{y^2}\right). \tag{30}$$

We may further incorporate the tHiggs couplings to gg and $\gamma\gamma$ generated at the one-loop level,

$$\mathcal{L}_{h_t^0}^{gg,\gamma\gamma} = (g_{hgg} + \Delta g_{hgg}^{(t')})\frac{\alpha_s}{16\pi v_{\rm EW}} h_t^0 G^{\mu\nu} G_{\mu\nu} + (g_{h\gamma\gamma} + \Delta g_{h\gamma\gamma}^{(t')})\frac{\alpha}{8\pi v_{\rm EW}} h_t^0 F^{\mu\nu} F_{\mu\nu}, \tag{31}$$

where $\alpha_s \equiv g_s^2/(4\pi)$ with g_s being the $SU(3)_c$ gauge coupling and $\alpha \equiv e^2/(4\pi)$ with e being the electromagnetic coupling. The coefficients g_{hgg}, $\Delta g_{hgg}^{(t')}$, $g_{h\gamma\gamma}$, and $\Delta g_{h\gamma\gamma}^{(t')}$ in Eq. (31) are

$$g_{hgg} = \sum_f g_{hff} A_{1/2}^h(\tau_f), \tag{32}$$

$$\Delta g_{hgg}^{(t')} = \frac{4}{3}\sin^2\theta\left(\frac{y_{\chi t}}{y}\right)^2\left[1 + \mathcal{O}\left(\frac{y_{\chi t}}{y}\right)^2\right], \tag{33}$$

$$g_{h\gamma\gamma} = g_{hVV} A_1(\tau_W) + \sum_f N_c^{(f)} Q_f^2 g_{hff} A_{1/2}^h(\tau_f), \tag{34}$$

$$\Delta g_{h\gamma\gamma}^{(t')} = \frac{16}{9}\sin^2\theta\left(\frac{y_{\chi t}}{y}\right)^2\left[1 + \mathcal{O}\left(\frac{y_{\chi t}}{y}\right)^2\right], \tag{35}$$

where $N_c^{(f)} = 3(1)$ for quarks (leptons), $\tau_i \equiv 4m_i^2/m_h^2$, and the functions $A_1(x)$ and $A_{1/2}^h(x)$ are defined as

$$A_1(x) = 2 + 3x + 3x(2-x)f(x), \tag{36}$$

$$A_{1/2}^h(x) = 2x[1 + (1-x)f(x)], \tag{37}$$

$$f(x) = \begin{cases} [\arcsin(1/\sqrt{x})]^2 & \text{for } x > 1 \\ -\frac{1}{4}\left[\ln\frac{1+\sqrt{1-x}}{1-\sqrt{1-x}} - i\pi\right]^2 & \text{for } x \le 1 \end{cases}. \tag{38}$$

Note the terms in Eqs. (33) and (35) corresponding to the nondecoupling contributions from integrating out the t' quark. However, the t' contributions are numerically negligible since the overall factor $\sin^2\theta$ turns out to be constrained by the Higgs coupling measurement as $\sin\theta \lesssim 0.2 - 0.4$ [see Eqs. (40) and (42), and this is also the case for A_t^0 as will be seen later]. Thus, the $h_t^0 - g - g$ and $h_t^0 - \gamma - \gamma$ couplings approximately become the same as those of the SM Higgs boson. Note that the *CP*-odd top-mode pNGB A_t^0 is necessarily heavier than the tHiggs [see Eqs. (10), (24) and (25)]; hence, the tHiggs cannot decay to A_t^0. Therefore, both the production cross sections and decay properties of h_t^0 are almost the same as those of the SM Higgs boson, up to some size of a deviation controlled by a coupling parameter $\cos\theta$.

B. Fitting the tHiggs couplings to the LHC Run-I data

The ATLAS [14–18] and CMS [19–24] collaborations have provided the signal strengths $\hat{\mu}$ of the 126 GeV Higgs boson for each decay channel, which are classified by the production processes; gluon-gluon fusion (ggF) plus top-quark associate productions ($t\bar{t}H$), $\hat{\mu}(\text{ggF} + t\bar{t}\text{H})$; and vector-boson fusion (VBF) plus vector-boson associate productions (VH), $\hat{\mu}(\text{VBF} + \text{VH})$.[3] In Table I, we present the signal strengths reported by the ATLAS and CMS

[3]As noted around Eq. (22), the *CP*-odd top-mode pNGB A_t^0 does not interfere the Higgs search in the VH channel because of no couplings to light quarks, in sharp contrast to other *CP*-odd Higgs like those in the 2HDM. This makes it possible to directly quote the Higgs coupling data from the VH channel to constrain solely the tHiggs without resonance contributions of *CP*-odd Higgs bosons.

TABLE I. The best-fit signal strengths $\hat{\mu}(\mathrm{ggF}+\mathrm{t\bar{t}H})$ and $\hat{\mu}(\mathrm{VBF}+\mathrm{VH})$ reported from the Higgs search at the ATLAS [14–18] and CMS [19–24] experiments. As for the WW^* channel (CMS), the value of $\hat{\mu}(\mathrm{ggF}+\mathrm{t\bar{t}H})$ is taken from Ref. [21], and the value of $\hat{\mu}(\mathrm{VBF}+\mathrm{VH})$ is from Ref. [22]. The value of $\hat{\mu}(\mathrm{ggF}+\mathrm{t\bar{t}H})$ for the $\tau\tau$ channel (CMS) is quoted from the one-jet result in Ref. [23].

Decay channel	$\hat{\mu}(\mathrm{ggF}+\mathrm{t\bar{t}H})$	$\hat{\mu}(\mathrm{VBF}+\mathrm{VH})$	$\Delta\mu(\mathrm{ggF}+\mathrm{t\bar{t}H})$	$\Delta\mu(\mathrm{VBF}+\mathrm{VH})$	Ref.
$\gamma\gamma$ (ATLAS)	1.6	1.7	0.25	0.63	[14]
ZZ^* (ATLAS)	1.8	1.2	0.35	1.30	[15]
WW^* (ATLAS)	0.82	1.66	0.36	0.79	[16]
$\tau\tau$ (ATLAS)	1.1	1.6	1.16	0.75	[17]
$b\bar{b}$ (ATLAS)	⋯	0.2	⋯	0.64	[18]
$\gamma\gamma$ (CMS)	0.52	1.48	0.60	1.33	[19]
ZZ^* (CMS)	0.9	1.0	0.45	2.35	[20]
WW^* (CMS)	0.72	0.62	0.37	0.53	[21,22]
$\tau\tau$ (CMS)	1.07	0.94	0.46	0.41	[23]
$b\bar{b}$ (CMS)	⋯	1.0	⋯	0.5	[24]

collaborations. By using them, we construct a simple χ^2 function as

$$\chi^2(\theta) \equiv \sum_X \sum_{C,i,j} \left(\frac{\mu_i^X(\theta) - \hat{\mu}_{C,i}^X}{\Delta\mu_{C,i}^X} \right)^2, \tag{39}$$

where $\mu_i^X(\theta)$ implies the signal strength of tHiggs for each production channel $i,j \in \{\mathrm{ggF}+\mathrm{t\bar{t}H}, \mathrm{VBF}+\mathrm{VH}\}$ and each decay channel $X \in \{\gamma\gamma, ZZ^*, WW^*, \tau\tau, b\bar{b}\}$. We use $G_F = 1.166\times10^{-5}\,\mathrm{GeV}^{-2}$, $m_Z = 91.188$ GeV, $\alpha = 1/137$, $m_t = 173.1$ GeV, and $\alpha_s(m_Z) = 0.118$ as inputs [25]. Then, the signal strength of the tHiggs depends only on $\cos\theta$, which parametrizes couplings between tHiggs and SM particles as seen from Eqs. (28), (29), and (30). $\hat{\mu}_{C,i}^X$ is the value of the best-fit signal strength of the 126 GeV Higgs for each production (i) and decay channel (X) reported by the experiments $C \in \{\mathrm{ATLAS}, \mathrm{CMS}\}$. We may take into account the next-to-leading-order corrections to the ggF process arising from QCD, the so-called K-factor, for the CP-even scalar [26], $K_h^g = 1 + (215/12)\alpha_s(m_h)/\pi$, where $\alpha_s(m_h)$ is the one-loop QCD gauge coupling at the scale $\mu = m_h$. In the left panel of Fig. 1 (solid curve), we show $\Delta\chi^2 \equiv \chi^2 - \chi^2_{\mathrm{min}}$ as a function of $\cos\theta$, where $\chi^2_{\mathrm{min}} = 13.5$ at $\cos\theta = 1$ for the number of degrees of freedom being 18. From the left panel, we find the 95% C.L. allowed region for $\cos\theta$:

$$0.97 \le \cos\theta \le 1. \tag{40}$$

Using the mass relation between $m_{h_t^0}^{(0)}$ and $m_{A_t^0}^{(0)} \simeq m_{A_t^0}$ given in Eq. (10) with Eq. (26) taken into account, from Eq. (40), we may place an indirect bound on the mass of A_t^0. In the right panel of Fig. 1, we plot $m_{A_t^0}$ as a function of $\cos\theta$, from which the 95% C.L. allowed region of $m_{A_t^0}$ (horizontal solid line) reads

$$m_{A_t^0} \ge 923\ \mathrm{GeV}. \tag{41}$$

We may take into account the correlation between $\hat{\mu}(\mathrm{ggF}+\mathrm{t\bar{t}H})$ and $\hat{\mu}(\mathrm{VBF}+\mathrm{VH})$, which can be read off from Ref. [27], though it is not in public. The 95% C.L. allowed region in Eqs. (40) and (41) would then change to

$$0.91 \le \cos\theta \le 1 \tag{42}$$

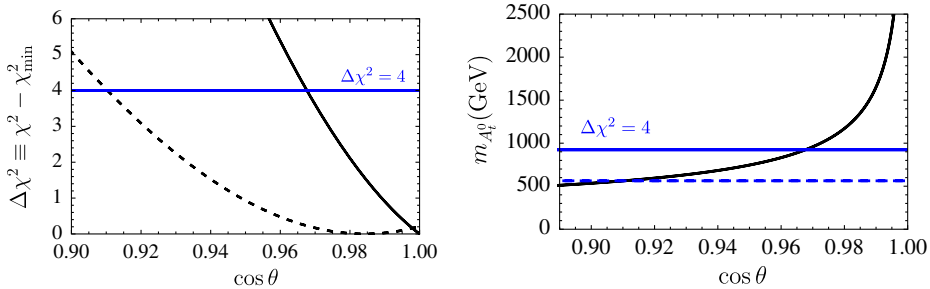

FIG. 1 (color online). The plots of $\Delta\chi^2 \equiv \chi^2 - \chi^2_{\mathrm{min}}$ (left panel) and $m_{A_t^0}$ (right panel) as a function of $\cos\theta$ together with the 95% C.L. upper limits represented by the $\Delta\chi^2 = 4$ lines. In the left panel, the dashed and solid curves have, respectively, been created by the χ^2 goodness-of-fit tests with and without the incorporation of the correlation mentioned in the text. In the right panel, the cross points made of the black-solid curve with blue-dashed and blue-solid horizontal lines correspond to the 95% C.L. lower limits given in Eq. (40) [or Eq. (41)] and Eq. (42) [or Eq. (43)], respectively.

for $\cos\theta$ and (see the horizontal dashed line in the right panel of Fig. 1)

$$m_{A_t^0} \geq 563 \text{ GeV} \tag{43}$$

for $m_{A_t^0}$. Thus, the incorporation of the correlation would make the lower bounds on $(\cos\theta, m_{A_t^0})$ milder. In the present study, therefore, we shall explore the LHC phenomenology of A_t^0 by scanning the mass in the high-mass range [Eq. (41)] and the low-mass range [Eq. (43)].

IV. *CP*-ODD TOP-MODE pNGB (A_t^0) AT THE LHC

In this section, we explore the LHC phenomenologies of A_t^0 to compare the predicted A_t^0 signals in several decay channels with the currently available data searching for new resonances provided from LHC Run-I.

A. A_t^0 coupling properties

We start with reading off the relevant A_t^0 interaction terms from the Lagrangian Eq. (23):

$$\begin{aligned}\mathcal{L}_{A_t^0} = &-i\left(\frac{\sin^3\theta}{\cos\theta}\right)\frac{m_t}{v_{\rm EW}}A_t^0\bar{t}\gamma_5 t - \frac{3\sin\theta\cos^2\theta}{4v_{\rm EW}}[z_t^0\partial_\mu A_t^0\partial^\mu h_t^0 \\ &- h_t^0\partial_\mu A_t^0\partial^\mu z_t^0 - 2((m_{A_t^0}^{(0)})^2\sin^2\theta)A_t^0 h_t^0 z_t^0] \\ &+ \frac{3\sin^3\theta}{4v_{\rm EW}}[A_t^0\partial_\mu z_t^0\partial^\mu h_t^0 - h_t^0\partial_\mu A_t^0\partial^\mu z_t^0].\end{aligned} \tag{44}$$

Note that all the A_t^0 couplings vanish when $\sin\theta = v_{\rm EW}/f \simeq m_{h_t^0}^{(0)}/m_{A_t^0}$ is sent to zero with $v_{\rm EW} \simeq 246$ GeV or $m_{h_t^0}^{(0)} \simeq 230$ GeV fixed. This should be so since A_t^0 decouples from the low-energy effective theory in this limit, i.e., $m_{A_t^0} \simeq m_{A_t^0}^{(0)} \to \infty$. The overall suppression by this $\sin\theta$ also ensures the weakness of the A_t^0 couplings, leading to a quite small total width and giving the crucial difference between A_t^0 and other *CP*-odd scalars as in the MSSM/2HDM, as will be discussed below.

Note also the absence of couplings to ZZ and WW since A_t^0 is orthogonal to the would-be NGBs z_t^0 and $w_t^\pm$; actually, there exist terms coupling to the longitudinal mode of $W^\pm$ like $A_t^0 - w_t^- - w_t^+$, which, however, vanishes when the amplitude is evaluated at the A_t^0 mass on shell. Although not being displayed in Eq. (44), the $A_t^0 - Z - h_t^0$ term is also present in the Lagrangian Eq. (23), where the transverse component of Z does not contribute in the on-shell amplitude. This fact is closely tied with the Goldstone boson equivalence theorem. It thus turns out that the A_t^0 coupling to the weak gauge bosons relevant to the A_t^0 on-shell amplitude is allowed only by involving both the tHiggs h_t^0 and the longitudinal mode $Z_L \equiv z_t^0$, as presented in the second line of Eq. (44). Similar arguments are applicable to other *CP*-odd Higgs bosons, such as those in the MSSM/2HDM.

B. Decay properties of A_t^0

Using Eq. (44) and taking into account the loop-induced couplings to gg and $\gamma\gamma$, we compute the partial decay widths of A_t^0 relevant to the two-body decay processes to obtain

$$\Gamma(A_t^0 \to t\bar{t}) = \frac{\sqrt{2}G_F N_c m_t^2 m_{A_t^0}}{8\pi^2}\left(\frac{\sin^3\theta}{\cos\theta}\right)^2 \cdot \beta_A(m_t), \tag{45}$$

$$\begin{aligned}\Gamma(A_t^0 \to gg) = &\frac{\sqrt{2}G_F\alpha_s^2 m_{A_t^0}^3}{128\pi^3} \\ &\cdot \left|\left(\frac{\sin^3\theta}{\cos\theta}\right)A_{1/2}^A(\tau_t) + 2(\sin\theta\cos\theta)\right|^2,\end{aligned} \tag{46}$$

$$\begin{aligned}\Gamma(A_t^0 \to \gamma\gamma) = &\frac{\sqrt{2}G_F\alpha^2 m_{A_t^0}^3}{256\pi^3} \\ &\cdot \left|\left(\frac{\sin^3\theta}{\cos\theta}\right)N_c Q_t^2 A_{1/2}^A(\tau_t) + \frac{8N_c}{9}(\sin\theta\cos\theta)\right|^2,\end{aligned} \tag{47}$$

$$\begin{aligned}\Gamma(A_t^0 \to Z_L h_t^0) = &\frac{9\sqrt{2}G_F m_{A_t^0}^3}{256\pi}\sin^2\theta\cdot\beta_A(m_{h_t^0}) \\ &\times\left[\left(\sin^2\theta - \frac{m_{h_t^0}^2}{m_{A_t^0}^2}\right)(\cos^2\theta - \sin^2\theta)\right. \\ &\left. + \frac{m_Z^2}{m_{A_t^0}^2}\cos^2\theta\right]^2,\end{aligned} \tag{48}$$

where $A_{1/2}^A(x) = 2xf(x) \to 2(x \gg 1)$ with $f(x)$ being defined in Eq. (38) and

$$\beta_A(m_t) \equiv \sqrt{1 - \frac{4m_t^2}{m_{A_t^0}^2}}, \tag{49}$$

$$\beta_A(m_{h_t^0}) \equiv \sqrt{\left[1 - \frac{(m_{h_t^0} - m_Z)^2}{m_{A_t^0}^2}\right]\left[1 - \frac{(m_{h_t^0} + m_Z)^2}{m_{A_t^0}^2}\right]}. \tag{50}$$

Note the second terms in Eqs. (46) and (47), coming from integrating out the t' quark. In Fig. 2, we plot the total decay width (blue-solid curve in the left panel) and branching ratios (right panel) of A_t^0 as a function of the parent particle mass $m = (m_{A_t^0}, m_{h_{\rm SM}})$ (bottom axis) and $\cos\theta$ (top axis) where $m_{A_t^0}(\simeq m_{A_t^0}^{(0)})$ and $\cos\theta$ are related to each other by the mass formula [Eq. (10)] with $m_{h_t^0}^{(0)} \simeq 230$ GeV fixed. As seen from the left panel, A_t^0 is still a narrow resonance even if the mass reaches the scale over 1 TeV, i.e., $\Gamma_{\rm tot}/m_{A_t^0} \ll 1$, where the $t\bar{t}$ mode rapidly damps as the mass increases. This happens due to the presence of the mass formula

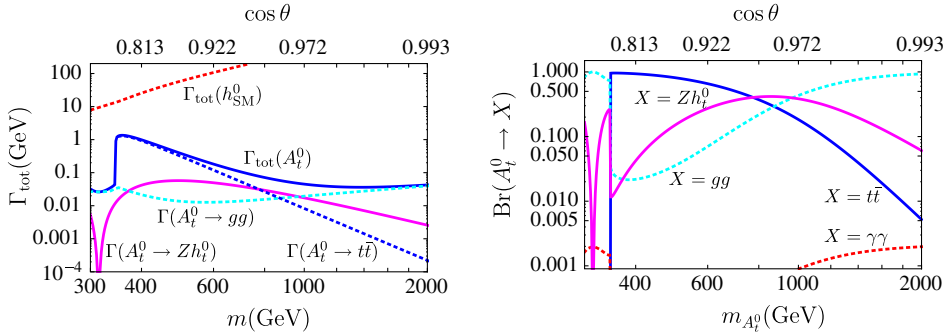

FIG. 2 (color online). Left panel: The total decay width of A_t^0 and the dominant partial widths. Right panel: The branching ratio of A_t^0. Both are represented as a function of the parent particle mass $m = (m_{h_t^0}, m_{h_{\rm SM}})$ (bottom axis) or $\cos\theta$ (top axis). In the left panel, the total decay width of the SM Higgs boson is shown for comparison.

[Eq. (10)], which significantly affects the mass dependence of the total width for the high-mass region; as the mass gets larger, the partial decay width for the $t\bar{t}$ mode goes like $\sim 1/m_{A_t^0}^5$, due to the high suppression by the overall coupling $\sim(\sin^3\theta)^2$ [see Eq. (45)], where $\sin\theta$ has been replaced by $m_{h_t^0}^{(0)}/m_{A_t^0} \simeq (230\ \text{GeV})/m_{A_t^0}$. The total width is then governed by the gg mode, so that $\Gamma_{\rm tot}(A_t^0) \sim \Gamma(A_t^0 \to gg) \sim m_{A_t^0}^3 \tan^2\theta \sim m$, according to Eq. (48), which does not grow like $\sim m^3$ as in the case of the typical width of decays to spin-1 bosons. This is the salient feature of A_t^0 closely related to the fact that A_t^0 is the top-mode pseudo-boson partner of the Higgs h_t^0. In the left panel, the total width is also compared with that of the SM Higgs (red-dotted curve). This shows that A_t^0 is indeed a narrower resonance than the SM Higgs boson for the whole mass range. Note also the presence of a dip in the $A_t^0 \to Zh_t^0$ channel; this takes place when the terms in the square bracket of Eq. (48) vanish as

$$\left(\sin^2\theta - \frac{m_{h_t^0}^2}{m_{A_t^0}^2}\right)(\cos^2\theta - \sin^2\theta) + \frac{m_Z^2}{m_{A_t^0}^2}\cos^2\theta = 0$$
$$\leftrightarrow m_{A_t^0}^2 = \frac{(m_{h_t^0}^{(0)})^2(m_Z^2 + 2(m_{h_t^0}^{(0)})^2 - 2m_{h_t^0}^2)}{(m_{h_t^0}^{(0)})^2 - m_{h_t^0}^2 + m_Z^2} \simeq (310\ \text{GeV})^2, \tag{51}$$

where we used the tree-level mass formula [Eq. (10)] with $m_{h_t^0}^{(0)} \simeq 230$ GeV, the one-loop mass $m_{h_t^0} = 126$ GeV, and $m_Z \simeq 90$ GeV.

The right panel of Fig. 2 combined with the indirect limits on $m_{A_t^0}$ in Eqs. (41) and (43) imply that the accessible decay channels of A_t^0 at the LHC can be $A_t^0 \to t\bar{t}, gg, Zh_t^0$:

(i) First is the high-mass case with $m_{A_t^0} \geq 1$ TeV indicated from the limit in Eq. (41) (hereafter, we shall call this A_t^0 "high-mass A_t^0"), where the $A_t^0 \to gg$ mode will be the expected discovery channel at the LHC, which is accessible in a way similar to searches for new heavy bosons mainly decaying to gluon jets [28];

(ii) Second is the low-mass case with $563\text{GeV} \leq m_{A_t^0} \leq 1\text{TeV}$ indicated from the limit in Eq. (43), where the $A_t^0 \to Zh_t^0$ mode will be expected as the discovery channel at the LHC, which can be seen in the same way as searches for other CP-odd Higgs bosons in the extended Higgs sector as in the MSSM/2HDM through the decay to Zh^0 [29] (this A_t^0 will be called "low-mass A_t^0"). Note that the A_t^0 still emerges as the narrow resonance in the Zh channel (see the left panel of Fig. 2), compared to other CP-odd scalars, like A^0 in the MSSM/2HDM, which becomes a quite broader resonance with the total width of $\mathcal{O}(100)$ GeV in this mass range [30]. Thus, A_t^0 can be distinguished from A^0 in the MSSM/2HDM at the LHC. This is mainly due to the presence of the intrinsic mass formula [Eq. (10)], which is absent in the MSSM/2HDM, as emphasized above.

The predicted signals of A_t^0 through these decay channels compared with current LHC limits will be discussed later.

C. Production cross sections of A_t^0

The branching fraction in the right panel of Fig. 2 implies that at the LHC A_t^0 is mainly produced through the ggF or top-quark associate process ($t\bar{t}A$) like the $t\bar{t}H$ production for the SM Higgs. To make a quantitative argument, it is convenient to evaluate the cross section $gg/t\bar{t} \to A_t^0$ by normalizing it with the corresponding cross section for the SM Higgs:

$$\sigma(gg/t\bar{t} \to A_t^0) = \sigma(gg/t\bar{t} \to h_{\rm SM}^0) \times \frac{\sigma(gg/t\bar{t} \to A_t^0)}{\sigma(gg/t\bar{t} \to h_{\rm SM}^0)}. \tag{52}$$

In Fig. 3, we plot the ratio $\sigma(gg/tt \to A_t^0)/\sigma(gg/tt \to h_{\rm SM}^0)$ as a function of the produced particle mass

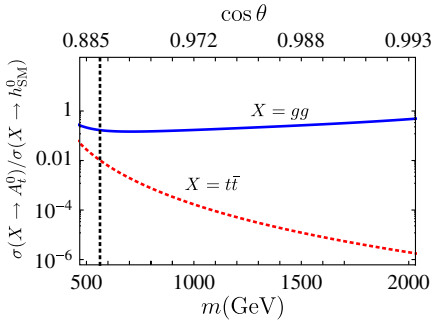

FIG. 3 (color online). The ratios of the production cross sections $\sigma(t\bar{t} \to A_t^0)/\sigma(t\bar{t} \to h_{\rm SM}^0)$ (red dotted curve) and $\sigma(gg \to A_t^0)/\sigma(gg \to h_{\rm SM}^0)$ (blue solid curve) as a function of the produced particle mass $m = (m_{A_t^0}, m_{h_{\rm SM}})$ (bottom axis) or $\cos\theta$ (top axis). The vertical dotted line corresponds to the indirect mass limit in Eq. (43).

$m = (m_{A_t^0}, m_{h_{\rm SM}})$. The mass range analyzed here has been restricted to 563 GeV $\leq m \leq$ 2000 GeV, which is indicated from the indirect mass limits in Eqs. (41) and (43).

From Fig. 3, one can see that the $t\bar{t}A$ production is suppressed compared to the SM Higgs case for the mass range constrained by the indirect limits in Eqs. (41) and (43). The ggF production is somewhat suppressed compared to the SM Higgs one, which is due to the numerical suppression by the overall coupling, $g_{A_t^0 gg} \propto 2(2)^2 \tan^2\theta$ (in the heavy quark limit), when we take $\cos\theta \sim 1$ to be consistent with the indirect limits. Since the ggF production is much larger than the $t\bar{t}H$ production in the case of the SM Higgs boson, the ggF production of the A_t^0 is highly dominant enough to neglect the $t\bar{t}A$ production at the LHC.

D. Current LHC limits on high-mass A_t^0

We shall discuss the current LHC limits on the high-mass A_t^0 (1 TeV $\leq m_{A_t^0} \leq$ 2 TeV) in comparison with the available data on searches for new resonances at LHC Run-I. We focus on the A_t^0 signals produced via the ggF decaying to $t\bar{t}$ and gg. Figure 4 shows the plots of the production cross section times branching ratio $\sigma \times {\rm Br}(A_t^0 \to gg/t\bar{t})$, as a function of $m_{A_t^0}$ in units of fb. In the figure the observed 95% C.L. upper limits for each channel have also been plotted, which are quoted from Refs. [28,31,32]. More on details of the comparison with those data have been given in the caption of Fig. 4. In computing the ggF production cross section $\sigma(gg \to A_t^0)$, we have used the CTEQ6M [33] for the parton distribution function. Here, we have taken into account the K factor for the ggF production of CP-odd scalars with the mass m_A, $K_A^g = 1 + (69/4)\alpha_s(m_A)/\pi$ [26]. Figure 4 implies that the high-mass A_t^0 has not severely been constrained yet by the LHC Run-I data.

It is anticipated that the upcoming LHC Run-II will provide more stringent constraints or a hint for the discovery of A_t^0. In particular, the searches for CP-odd scalars decaying to $t\bar{t}$ and gg would be interesting and challenging to probe the high-mass A_t^0 around a few TeV, which has not so far been performed. The characteristic feature of A_t^0 would be seen as "a quite narrow resonance" with $\Gamma_{\rm tot} \ll m_{A_t^0}$ in the $t\bar{t}$ and gg mass distributions, as is indicated from the left panel of Fig. 2.

E. Current LHC limits on low-mass A_t^0

We next discuss the LHC discovery channel of the low-mass A_t^0 (563 GeV $\leq m_{A_t^0} \leq$ 1 TeV). In the case of the low-mass A_t^0, one can see from Fig. 2 that an interesting channel is the $A_t^0 \to Zh_t^0$ having the branching ratio ${\rm Br}(A_t^0 \to Zh_t^0) = 20 - 40\%$, which would be large enough to be accessible at the LHC.

In the left panel of Fig. 5, we make a plot of the production cross section times the branching ratio of A_t^0 for the Zh_t^0 channel, $\sigma \times {\rm Br}(A_t^0 \to Zh_t^0)$, as a function of $m_{A_t^0}$ in units of pb, together with the observed limit from the currently available data on searches for extended Higgs sectors by the CMS experiments at $\sqrt{s} = 8$ TeV with $\mathcal{L} =$ 19.5 fb^{-1} [29]. Here, we have allowed a light A_t^0 having the

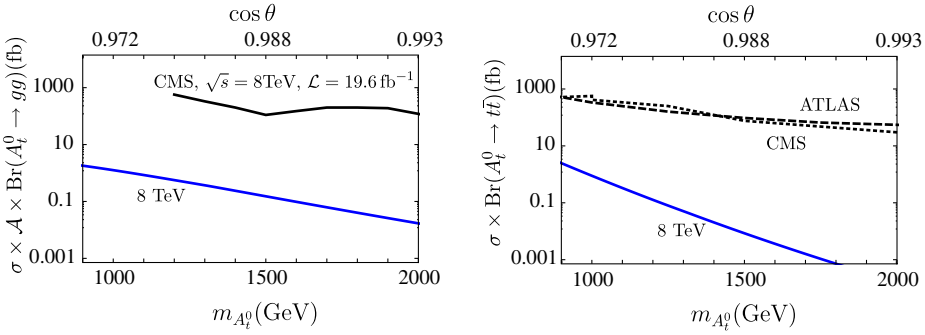

FIG. 4 (color online). The cross sections, $\sigma(gg \to A_t^0) \times {\rm Br}(A_t^0 \to gg)$ (left panel) and $\sigma(gg \to A_t^0) \times {\rm Br}(A_t^0 \to t\bar{t})$ (right panel), as a function of $m_{A_t^0}$ in units of fb. In the left panel, the observed 95% C.L. upper limit (black solid curve) is quoted from data on searches for new resonances in dijet mass distribution of gluon-gluon type by the CMS experiments at $\sqrt{s} = 8$ TeV with $\mathcal{L} = 19.6$ fb^{-1} [28], where $\mathcal{A}$ denotes the acceptance, $\mathcal{A} = 0.6$, which is read off from the reference. In the right panel, the observed 95% C.L. upper limit from searches for Z' resonance with $\Gamma_{Z'}/M_{Z'} = 1.2\%$ by the ATLAS experiments at $\sqrt{s} = 8$ TeV with $\mathcal{L} = 14$ fb^{-1} data [31] (black dashed curve) and the CMS experiments at $\sqrt{s} = 8$ TeV with $\mathcal{L} = 19.7$ fb^{-1} data [32] (black dotted curve) are also shown.

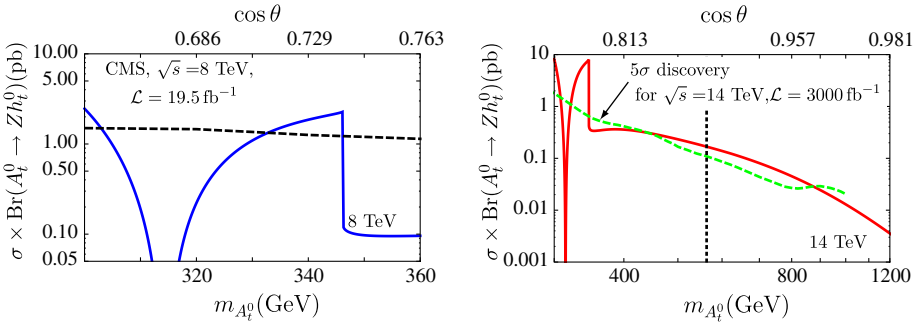

FIG. 5 (color online). Left panel: The plot of $\sigma_{\rm ggF}(pp \to A_t^0) \times {\rm Br}(A_t^0 \to Zh_t^0)$ as a function of $m_{A_t^0}$ in units of pb for a low-mass range $m_{A_t^0}(m_{A_t^0} \leq 360$ GeV). The observed 95% C.L. upper limit from data on searches for extended Higgs sectors by the CMS experiments at $\sqrt{s} = 8$ TeV with $\mathcal{L} = 19.5$ fb^{-1} [29] has also been shown by the black dashed curve. Right panel: The expected signal strength of $\sigma_{\rm ggF}(pp \to A_t^0) \times {\rm Br}(A_t^0 \to Zh_t^0)$ at the 14 TeV LHC for a mass range $m_{A_t^0} \leq 1$ TeV (red solid curve). Also, the curve corresponding to the 5σ discovery at $\mathcal{L} = 3000$ fb^{-1} provided by the CMS simulation [34] (green dashed curve) has been displayed. The vertical dotted line corresponds to the indirect mass limit in Eq. (43).

mass slightly off from the indirect limit in Eq. (43), since the current LHC bound has not reached a higher-mass region such as $m_A \geq 563$ GeV. The current limit requires the low-mass A_t^0 to have

$$303\ {\rm GeV} \leq m_{A_t^0} \leq 333\ {\rm GeV} \quad {\rm or} \quad 2m_t \simeq 346\ {\rm GeV} \leq m_{A_t^0}, \tag{53}$$

in which the latter case is consistent with the indirect limit in Eq. (43). The small allowed window for a low-mass region $(303\ {\rm GeV} \leq m_{A_t^0} \leq 333\ {\rm GeV})$ has been present because of the dip in Eq. (48) [see Eq. (51)].

The A_t^0 branching ratio for the Zh_t^0 mode is comparable with the branching ratio of the CP-odd Higgs boson (A^0) decaying to Zh^0 in the MSSM/2HDM with $\tan\beta = 3$ [26], so it is interesting to compare these signals at the same mass. It turns out that the production cross section of A_t^0 is actually larger than that of A_t^0 in the MSSM/2HDM for the low-mass region; indeed, the ratio of the ggF production cross sections of A_t^0 to that of A^0 evaluated at the same mass goes like

$$\frac{\sigma(gg \to A_t^0)}{\sigma(gg \to A^0)} \simeq \frac{2\tan^2\theta}{\cot^2\beta}, \tag{54}$$

where the heavy quark mass limit $m_t \to \infty$ has been taken. Taking $m_{A_t^0} = 600$ GeV as a sample benchmark point for the low-mass A_t^0, we may numerically estimate the ratio in Eq. (54) to get

$$\frac{\sigma(gg \to A_t^0)}{\sigma(gg \to A^0)} \simeq 3.2 \qquad {\rm for}\ \tan\beta = 3. \tag{55}$$

This implies that the search for A_t^0 would be more accessible than A^0 through the Zh^0 channel; the discovery of A_t^0 would be possible earlier than that of A^0.

In light of the LHC experiment with the high statistics, in the right panel of Fig. 5, we plot $\sigma_{\rm ggF} \times {\rm Br}(A_t^0 \to Zh_t^0)$ as a function of $m_{A_t^0}$ in units of pb at $\sqrt{s} = 14$ TeV (red solid curve). Also, the 5σ discovery potential (green dashed curve) for pNGB scalars in the Zh channel at $\mathcal{L} = 3000$ fb^{-1} provided from the CMS simulation [34] has been shown. From the right panel of Fig. 5, we see that the low-mass A_t^0 with the mass in a range

$$563\ {\rm GeV} \leq m_{A_t^0} \leq 875\ {\rm GeV} \tag{56}$$

is expected to be discovered at the upcoming LHC experiments.

V. SUMMARY

In summary, we discussed the LHC phenomenologies of the top-mode pNGBs, h_t^0 (CP-even scalar, tHiggs), and A_t^0 (CP-odd scalar), arising as composite pNGBs in the model recently proposed in a framework of the top-quark condensation. We first analyzed the tHiggs h_t^0 couplings to the SM particles to compare them with the currently available data on the Higgs coupling measurements at the LHC. It was shown that the tHiggs can be consistent with the 126 GeV Higgs boson, allowing the amount of deviation controlled by a model parameter $\cos\theta \geq 0.91$ at 95% C.L. [Eq. (42)]. The bound on $\cos\theta$ was converted into an indirect limit on the mass of the CP-odd top-mode pNGB A_t^0 through the top-mode pNGB mass formula [Eq. (10)], leading to the lower bound $m_{A_t^0} \geq 563$ GeV [Eq. (43)].

We explored the direct searches for A_t^0 at the LHC by explicitly calculating the relevant production cross sections and partial decay widths. The total width of A_t^0 was shown to be quite smaller than that of the SM Higgs boson and other CP-odd scalars like A^0 as in the MSSM/2HDM (left panel of Fig. 2). This feature is still operative even for a high-mass region $m_{A_t^0} > 1$ TeV. This is essentially due to the intrinsic feature of the top-mode pNGBs characterized by the mass formula [Eq. (10)], which allows us to express

the overall coupling of A_t^0, $\sin\theta$, in terms of $1/m_{A_t^0}$, leading to the significant suppression of the total width in the high-mass region; in that sense, the weak coupling nature of A_t^0 is ensured by the mass formula. The branching fraction of A_t^0 was discussed by dividing into two cases (right panel of Fig. 2): (i) high-mass A_t^0 with $m_{A_t^0} \geq 1$ TeV, where A_t^0 decays to the digluon (∼63%) and A_t^0 decays to the tHiggs associated with the Z boson (∼16%) for $m_{A_t^0} \simeq 1.2$TeV, and (ii) low-mass A_t^0 with the mass in the range 563 GeV $\leq m_{A_t^0} \leq 1$ TeV, where A_t^0 mainly decays to $t\bar{t}$ (∼66%) and the tHiggs associated with the Z boson (∼27%) for $m_{A_t^0} = 600$ GeV. It was also found that the LHC production of A_t^0 is highly dominated by the ggF process for both the low-mass and high-mass cases (Fig. 3).

We then placed the current LHC limit on $m_{A_t^0}$ by using the currently available data on searches for new resonances in several channels (Fig. 4 and the left panel of Fig. 5) to find that all the direct limits are weaker than the indirect limit from the Higgs coupling measurements [Eq. (43)].

In light of the upcoming LHC experiment with higher statistics, the searches for CP-odd scalars decaying to $t\bar{t}/gg$ would be interesting and challenging to probe the A_t^0 with the mass $m_{A_t^0} \geq 1$ TeV, which has not so far been performed. The characteristic feature of A_t^0 would be seen as a quite narrow resonance with $\Gamma_{\rm tot} \simeq 0.1$ GeV in the $t\bar{t}/gg$ mass distribution (left panel of Fig. 2). Or a somewhat light A_t^0 with the mass in a range of 563 GeV $\leq m_{A_t^0} \leq 1$ TeV is expected to be observed as a quite narrow resonance in the channel decaying to Zh^0 produced from the ggF process. Such a light A_t^0 could be observed earlier than other CP-odd scalars such as A^0 in the MSSM/2HDM, due to the larger ggF production cross section [Eq. (55)]. We examined the discovery potential of the low-mass A_t^0 decaying into the Zh_t^0 at the 14 TeV LHC (right panel of Fig. 5). A light A_t^0 with the mass in a range 563 GeV $\leq m_{A_t^0} \leq 875$ GeV can be discovered at the 5σ level with $\mathcal{L} = 3000$ fb^{-1}.

More precise estimates on the A_t^0 discovery potential at LHC Run-II will be pursued in another publication.

Throughout the present paper, we have employed the nonlinear sigma model by integrating out the heavy Higgs boson H_t^0 at around $\mathcal{O}(1)$ TeV. One could also study the LHC phenomenology of the H_t^0 based on the linear sigma model, instead of the nonlinear realization. If one examines Appendix A of Ref. [9], one would notice that the H_t^0 with the mass of coupling property for the SM particles can be found just by rotating the tHiggs couplings by the angle θ, namely, replacing the overall angle $\cos\theta$ by $\sin\theta$. Taking into account the experimental constraint $\cos\theta \sim 1$, one would then find that all the production cross sections regarding the H_t^0 are suppressed by the overall factor of $\sin^2\theta$, compared to the SM-like Higgs case including the tHiggs. More precise arguments on this topic can be done in a way similar to the analyses on the top-Higgs boson as done in Refs. [35–37], which deserves another publication.

ACKNOWLEDGMENTS

This work was supported in part by the JSPS Grant-in-Aid for Scientific Research (S), Grant No. 22224003.

[1] G. Aad *et al.* (ATLAS), Phys. Lett. B **716**, 1 (2012).
[2] S. Chatrchyan *et al.* (CMS), Phys. Lett. B **716**, 30 (2012).
[3] V. Miransky, M. Tanabashi, and K. Yamawaki, Phys. Lett. B **221**, 177 (1989).
[4] V. Miransky, M. Tanabashi, and K. Yamawaki, Mod. Phys. Lett. A **04**, 1043 (1989).
[5] Y. Nambu, Report No. EFI-89-08.
[6] W. Marciano, Phys. Rev. Lett. **62**, 2793 (1989).
[7] W. J. Marciano, Phys. Rev. D **41**, 219 (1990).
[8] W. A. Bardeen, C. T. Hill, and M. Lindner, Phys. Rev. D **41**, 1647 (1990).
[9] H. S. Fukano, M. Kurachi, S. Matsuzaki, and K. Yamawaki, arXiv:1311.6629.
[10] H.-C. Cheng, B. A. Dobrescu, and J. Gu, arXiv:1311.5928.
[11] B. A. Dobrescu and C. T. Hill, Phys. Rev. Lett. **81**, 2634 (1998).
[12] R. S. Chivukula, B. A. Dobrescu, H. Georgi, and C. T. Hill, Phys. Rev. D **59**, 075003 (1999).
[13] Y. Nambu and G. Jona-Lasinio, Phys. Rev. **122**, 345 (1961).
[14] ATLAS Collaboration, Technical Report No. ATLAS-CONF-2013-012, 2013.
[15] G. Aad *et al.* (ATLAS Collaboration), Phys. Lett. B **726**, 88 (2013).
[16] ATLAS Collaboration, Technical Report No. ATLAS-CONF-2013-030, 2013.
[17] ATLAS Collaboration, Report No. ATLAS-CONF-2013-108; ATLAS CollaborationReport No. ATLAS-COM-CONF-2013-095.
[18] ATLAS Collaboration, Report No. ATLAS-CONF-2013-079; ATLAS CollaborationReport No. ATLAS-COM-CONF-2013-080.
[19] CMS Collaboration, Technical Report No. CMS-PAS-HIG-13-001, 2013.
[20] CMS Collaboration, Technical Report No. CMS-PAS-HIG-13-002, 2013.

[21] S. Chatrchyan *et al.* (CMS Collaboration), J. High Energy Phys. 01 (2014) 096.
[22] CMS Collaboration, Report No. CMS-PAS-HIG-13-022.
[23] S. Chatrchyan *et al.* (CMS Collaboration), J. High Energy Phys. 05 (2014) 104.
[24] S. Chatrchyan *et al.* (CMS Collaboration), Phys. Rev. D **89**, 012003 (2014).
[25] J. Beringer *et al.* (Particle Data Group), Phys. Rev. D **86**, 010001 (2012), and 2013 partial update for the 2014 edition.
[26] A. Djouadi, Phys. Rep. **457**, 1 (2008).
[27] A. Belyaev, M. S. Brown, R. Foadi, and M. T. Frandsen, arXiv:1309.2097.
[28] CMS Collaboration, Report No. CMS-PAS-EXO-12-059.
[29] CMS Collaboration, Report No. CMS-PAS-HIG-13-025.
[30] S. Kanemura, S. Moretti, Y. Mukai, R. Santos, and K. Yagyu, Phys. Rev. D **79**, 055017 (2009).
[31] ATLAS Collaboration, Report No. ATLAS-CONF-2013-052; ATLAS CollaborationReport No. ATLAS-COM-CONF-2013-052.
[32] S. Chatrchyan *et al.* (CMS Collaboration), Phys. Rev. Lett. **111**, 211804 (2013).
[33] J. Pumplin, D. Robert Stump, J. Huston, H.-L. Lai, P. Nadolsky, and W.-K. Tung, J. High Energy Phys. 07 (2002) 012.
[34] CMS Collaboration, Report No. CMS-PAS-HIG-13-024.
[35] R. S. Chivukula, C. Hoelbling, and N. J. Evans, Phys. Rev. Lett. **85**, 511 (2000).
[36] R. S. Chivukula, E. H. Simmons, B. Coleppa, H. E. Logan, and A. Martin, Phys. Rev. D **84**, 095022 (2011).
[37] R. S. Chivukula, P. Ittisamai, E. H. Simmons, B. Coleppa, H. E. Logan, A. Martin, and J. Ren, Phys. Rev. D **86**, 095017 (2012).